energy&fuels

pubs.acs.org/EF Article

Insight into the Oxidation Mechanism of a Cu-Based Oxygen Carrier (Cu → Cu_2O → CuO) in Chemical Looping Combustion

Chaohe Zheng, Jie Cao, Yongliang Zhang, and Haibo Zhao*

Cite This: *Energy Fuels* 2020, 34, 8718–8725 Read Online

ACCESS | Metrics & More | Article Recommendations

ABSTRACT: Cu-based materials have been regarded as suitable oxygen carrier (OC) candidates in chemical looping combustion as a result of their high reactivity. Because Cu is a common reduction product in the fuel reactor and can be reoxidized to CuO in the air reactor, obtaining insights into the complete oxidation process of Cu at a microcosmic level is critical for exploring the intrinsic oxidation mechanism and kinetics. In this work, the detailed oxidation steps have been investigated by density functional theory calculations. First, the most likely dissociative adsorption pathways of oxygen molecules on the Cu(111) surfaces are determined. On the basis of the Mulliken charge analysis and partial density of state analysis, the oxygen uptake process would preferentially produce a CuO nano-island rather than Cu_2O on the surface. Then, ions (O^{2-} and Cu^{2+}) diffusion pathways are examined to explore the details of oxide growth. Oxygen inward diffusion leads to the formation of Cu_2O, however with quite high energy barriers. On the contrary, the horizontal diffusion of copper atoms on the surface is quite easy in kinetics and thermodynamics, corresponding to an epitaxial growth of the CuO oxide nano-island and then the formation of an exterior thin CuO layer. Furthermore, the continuous outward diffusion (replenishing copper atoms for the epitaxial growth) of copper atoms in the Cu or Cu_2O bulk is also considered. Results show that the energy barrier of each diffusion step in the Cu(111) bulk is smaller than that in the Cu_2O(111) bulk, indicating that the bulk Cu_2O phase preferentially forms as a result of copper outward diffusion in the Cu(111) bulk and then is oxidized to generate the bulk CuO phase eventually. In such a way, a complete oxidation mechanism of Cu → Cu_2O → CuO is elucidated, which has been validated by a well-designed thermogravimetric experiment of controllable oxidation of pure copper.

1. INTRODUCTION

Chemical looping combustion (CLC),[1−4] which allows a sequestration-ready CO_2 stream to be directly generated from an innovative two-step reaction, has been raised as a promising carbon capture and storage (CCS) technology. There are two reactors in the chemical looping system, i.e., fuel reactor (FR) and air reactor (AR). It is well-known that the oxygen carrier (OC) is the key in CLC for its role of carrying active lattice oxygen and heat from the AR to the FR. The fuels are oxidized in the FR with the participation of active lattice oxygen of OCs, while at the same time, the OCs with high oxygen potential are reduced to the low-valence oxides or elementary substance. The reduced OCs are then transported to the AR, where they are reoxidized by air and regenerated back to high-valence oxides, liberating a large amount of heat. The regenerated metal oxides are recycled back to the FR for finalizing a loop. More than 700 OC materials have been examined in the literature.[5] Ni-, Fe-, Cu-, Mn-, and Co-based OC materials were widely tested in CLC.[6−10] As a common OC in CLC, CuO is reduced to Cu in the FR and then regenerates itself via Cu → Cu_2O → CuO in the AR, and the copper oxidation process (strong exothermic reaction) usually leads to an undesired sintering/agglomeration of Cu-based OC particles.[11−13] A fundamental understanding of the oxidation features will help to design high-performance and robust Cu-based OCs.

Until now, numerous experimental mechanism analyses have been conducted for exploring the oxidation characteristics of copper.[14−23] In the low-temperature region (350−550 °C), Park et al.[17] found that the surface reaction with the whisker formation on the outside was the dominant mechanism of copper oxidation. Mimura et al.[19] considered that the growth of Cu_2O predominated the oxidation in an intermediate temperature range (600−800 °C), including the lattice diffusion and the grain boundary diffusion, while the lattice diffusion would mainly contribute to the oxidation process at high temperatures (850−1050 °C) for a sharp disappearance of grain boundaries. Zhu et al.[18] reported that pure copper would produce both Cu_2O and CuO in an oxidation process, and the surface is always covered by a thin layer of cupric oxide before the complete consumption of metallic copper. They conjectured the oxidation mechanism in the further research[24] as follows: at the initial stage of the oxidation, the reaction 2Cu + O_2→ 2CuO on the gas−solid interface happens directly, and the later process is the formation of Cu_2O on the interface between Cu and CuO. However, these mechanisms are based on the microscopic experimental measurements, which cannot *in situ* monitor the distribution of oxides and the migration of

Received: March 26, 2020
Revised: May 8, 2020
Published: May 11, 2020

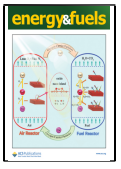

https://dx.doi.org/10.1021/acs.energyfuels.0c00941
Energy Fuels 2020, 34, 8718−8725

phase boundaries in the bulk. Therefore, an insight into the oxidation process of the Cu-based OC is highly desired.

As a consequence of the reaction mechanism, kinetics is an intuitional description. The previous conclusions of Cu oxidation kinetics are varied.[17−19,25−27] The mathematical models for oxidation rates based on the thickness of oxide as a function of time are always discrepant. Because it is intensively affected by the experimental environment, the length of the oxidation time, and the nature of the initial copper sample (size and single crystal or polycrystalline), it is hard to establish a consensus oxidation kinetic description. On the other side, although it is widely accepted[28] that the oxidation process of Cu_2O and Cu includes molecular oxygen adsorption, nucleation in the surface, and growth of the oxide, the underlying information is usually missing. Numerous studies[29−31] have pointed out that the growth of copper oxide is epitaxial across the surface and dominated by the outward diffusion of the cations. The existing works[32−36] mainly paid attention to the chemisorption and surface reconstruction processes at the initial stage of oxidation; however, they were rarely concerned about the O_2/substrate reaction itself and the details of crystalline island formation. In our recent research,[27] the oxidation mechanism and kinetics of reduction product Cu_2O in chemical looping with oxygen uncoupling (CLOU) have already been explored. However, it must be noted that there are two stages in the Cu oxidation process ($2Cu + 0.5O_2 \rightarrow Cu_2O$ and $Cu_2O + 0.5O_2 \rightarrow 2CuO$), and our previous study[27] has merely investigated the second oxidation stage ($Cu_2O + 0.5O_2 \rightarrow 2CuO$). The reliable oxidation mechanism of pure Cu is still ambiguous for its polyvalent transition ($Cu^0 \rightarrow Cu^+ \rightarrow Cu^{2+}$) in both the superficial layer and the bulk phase at an atomic layer. In this sense, there is an urgent need of more underlying information to clarify the various kinetics and ambiguous understanding of nucleation in copper oxidation.

The behavior of the OC in the AR is intrinsically dependent upon the electron and crystal structures of metal oxides. For example, the oxygen release rate of CuO is relatively stable in a CLOU experiment.[37] This is because the rate-limiting steps for CuO decomposition are the formation and desorption of O_2 according to the density functional theory (DFT) calculations, which are little affected by the conversion ratio. Through a theoretical study, it is found that the improvement of inert supports in sintering resistance is significantly influenced by the bond length and the adsorption energy between CuO and support materials.[38] An atomic modeling by the DFT method will effectively demonstrate the gas−solid reaction in a chemical looping process based on the detailed structure information and the energy profiles of every constituent elementary steps.[39,40] In this study, DFT calculations are used to investigate the Cu oxidation mechanism, including exploring the oxygen uptake pathways, the properties of products at the initial stage of Cu oxidation, and the atomic transport process that reflects the detailed nucleation information. This paper is a follow-up study to explore the oxidation mechanism of pure Cu, which will be beneficial to the holistic comprehension of the intrinsic reaction mechanism and kinetics of many multivalent oxides about the oxidation, sulfidation, and other reactions.

2. METHODS

2.1. DFT Calculations. In this study, the Cambridge Serial Total Energy Package (CASTEP)[41] program package is used for all DFT calculations, in which the generalized gradient approximation (GGA) in the form of Perdew−Wang (PW91) is chosen for the electron exchange−correlation energy. The interactions of electrons and ions are modeled by the ultrasoft pseudo-potential.[42] The Broyden−Fletcher−Goldfarb−Shanno (BFGS) method is used to search the lowest energy structure, and the cutoff energy is chosen as 400 eV. The Hubbard parameter U is introduced to describe the strong electron correlations of transition metals according to the well-known GGA + U method,[43] and 7.5 eV is set as a reasonable U value for the Cu 3d orbitals.[38,44] The van der Waals-inclusive correction (DFT-D) with the Ortmann−Bechstedt−Schmidt (OBS) method is applied for the DFT calculations. The Brillouin zone of the Cu bulk cell and the Cu(111) slabs are sampled with 8 × 8 × 8 and 4 × 4 × 1 Monkhorst−Pack k-point meshes, and the Brillouin zone of the Cu_2O bulk cell and the Cu_2O(111) slabs are sampled with 6 × 6 × 6 and 5 × 5 × 1 Monkhorst−Pack k-point meshes. The convergence criteria for total energy, maximum interatomic force, and displacement are 1.0×10^{-5} eV/atom, 0.03 eV/Å, and 0.001 Å, respectively.

As shown in Figure 1a, the bulk lattice parameters of Cu unit cells ($a = b = c = 3.606$ Å, and $\alpha = \beta = \gamma = 90°$) are in good agreement with the experimental values ($a = b = c = 3.604$ Å, and $\alpha = \beta = \gamma = 90°$).[45] As shown in Figure 1d, the bulk lattice parameters of Cu_2O unit cells ($a = b = c = 4.279$ Å, and 90°) are in good agreement with the experimental values ($a = b = c = 4.269$ Å, and $\alpha = \beta = \gamma = 90°$).[46] Additionally, as for the surface calculations, the six-layer p (3 × 3) Cu(111) (shown in Figure 1b) and p (2 × 1) Cu_2O(111) (shown in Figure 1e) surfaces are constructed, while the bottom three layers are fixed in the calculations. Meanwhile, the nine-layer p (3 × 3) Cu(111) (shown in Figure 1c) and p (1 × 1) Cu_2O(111) slabs (shown in Figure 1f) are applied for the bulk calculations, while the bottom two layers are fixed, and the top seven layers are relaxed. The vacuum space of 15 Å is added perpendicular to the surface, and all three-dimensional (3D) structures are put into periodic boundary conditions. For more details, please refer to our previous work.[27,44]

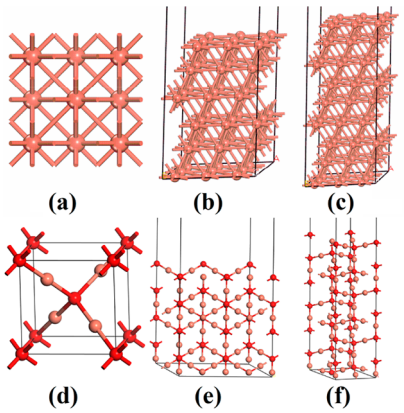

Figure 1. (a) Cu unit cell, (b) six-layer Cu(111) slab, (c) nine-layer Cu(111) slab, (d) Cu_2O unit cell, (e) six-layer Cu_2O(111) slab, and (f) nine-layer Cu_2O(111) slab (salmon pink ball, Cu; red ball, O).

In this study, the adsorption energy of the O_2 molecule on the surface, E_{ads}, is defined as

$$E_{ads} = E(O_2/slab) - E(O_2) - E(slab) \quad (1)$$

where $E(O_2)$ and E(slab) are the total energies of the free O_2 molecule and the bare slab, respectively, and $E(O_2/slab)$ presents the total energy of the adsorption structure. The complete linear/quadratic synchronous transit (LST/QST) approach[47] is used to find out the transition state (TS) as well as the energy barrier E_b, which is defined as

$$E_b = E(TS) - E(IS) \quad (2)$$

where E(TS) and E(IS) are the energies of the transition state and the initial state, respectively.

https://dx.doi.org/10.1021/acs.energyfuels.0c00941
Energy Fuels 2020, 34, 8718−8725

2.2. Experimental Approach. The OC samples used in this study are pure Cu ⟨111⟩ crystals (Hefei Kejing Materials Technology Co., China), which are in the shape of a square slice with 5 mm in length and 1 mm in thickness, as shown in Figure 2a. The purity of the samples reaches 99.9999%. The isothermal oxidation experiment is carried out in a synchronous thermal analyzer (SETARAM, France) at 600 °C. First the sample is heated to 600 °C with a constant rate of 20 K/min, while N_2 of 50 mL/min is used to sweep the sample. Next, a 20 vol % O_2/N_2 atmosphere is employed as the oxidizing agent for 10 h, and the gas flow rate is controlled at 50 mL/min by a mass flow meter/controller. After copper oxidation, the cross-section of the partially oxidized sample is cleaved within a resin cladding and characterized with scanning electron microscopy (SEM, ZEISS Gemini, Germany). Finally, the microstructure and elemental distribution of the partially oxidized sample (shown in Figure 2b) are characterized by an energy dispersive spectroscopy (EDS, ZEISS Gemini, Germany).

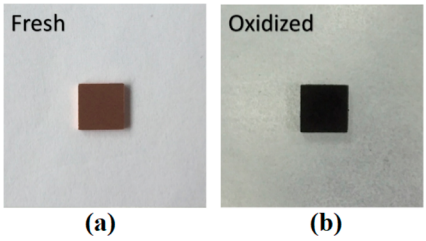

Figure 2. (a) Fresh copper specimens and (b) oxidized copper specimens after the oxidation experiment.

3. RESULTS AND ANALYSIS

3.1. Incipient Surface Oxidation of Cu(111): The Formation of the CuO Nano-island on the Surface. First, to find the potential adsorption sites, the oxygen molecule is placed toward the surface. On the Cu(111) surface, there are three kinds of potential adsorption sites [top site (labeled as T), bridge site (labeled as B), and hollow site (labeled as H)] for O_2 adsorption. Both vertical orientation (V) and horizontal orientation (H) are considered in this work. As shown in Figure 3, six structures of O_2 adsorptions are thus considered, while the geometric structure of "HT" means that O_2 horizontally adsorbs at the top site on the surface. After geometry optimization, as shown in Figure 3 (HH), the final stable construction of "HH" (O_2 horizontally adsorbs at the hollow site) shows the largest adsorption energy of −2.30 eV. Therefore, the structure of "HH" is regarded as the most stable adsorption, which has been set as the initial state of the surface oxidation [as shown in Figure 4 (IS)]. The length of the O−O bond is stretched to 1.522 Å (from 1.239 Å in the free molecule state), while the distance between the O_2 molecule and Cu surface is only 1.930 Å. To determine the favorable dissociation pathway of the oxygen molecule, two O atoms are moved along the horizontal direction as the O−O bond is broken and the stable dissociation configuration with the lowest overall energy is chosen as the final state (FS) of the incipient surface oxidation.

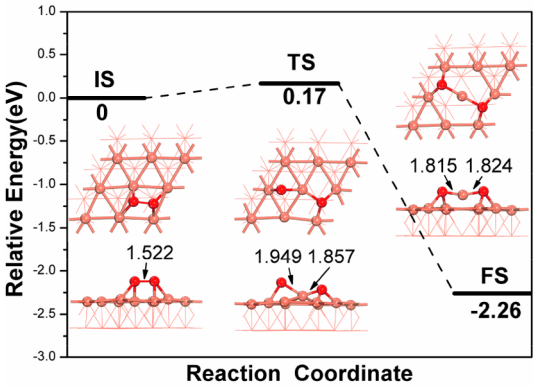

Figure 4. Pathway of O_2 dissociation on the perfect Cu(111) surface, combining the configuration evolution with the energy profile along the reaction coordinate.

As shown in Figure 4, the incipient surface oxidation process of Cu(111) can be summarized as below. Two oxygen atoms are induced to disperse to a closer position on the surface and bond with surrounding copper atoms gradually [Figure 4 (IS)]. Along with this process, a copper atom near the adsorption site is drawn away from the compact surface as a result of the attraction of the two oxygen atoms [Figure 4 (TS)], forming a horizontal O−Cu−O structure protruded from the surface [Figure 4 (FS)]. This structure, as a result of stress release in the top of the wetting layer, might induce the formation of the nano-island on the Cu(111) surface and then lead to an epitaxial growth of oxide. The O_2 dissociation process is exothermic with a reaction heat of −2.26 eV, and the energy barrier is only 0.17 eV, indicating that this dissociation is energy-favorable in both thermodynamics and kinetics, respectively.

To identify the components of the oxide nano-island, the partial density of states (PDOS) for three valence states of copper cations (Cu, Cu^{2+}, and Cu^{+}) is depicted in Figure 5. A similar peak appears near the Fermi level in both the oxidized copper cation on the Cu(111) surface [labeled by Cu@Cu(111), calculated above] and a Cu^{2+} cation in a complete CuO(111) surface [Cu@CuO(111), as a reference], and they also share a very similar peak shape around −2 eV, indicating that the electronic orbitals of Cu@Cu(111) are close to those

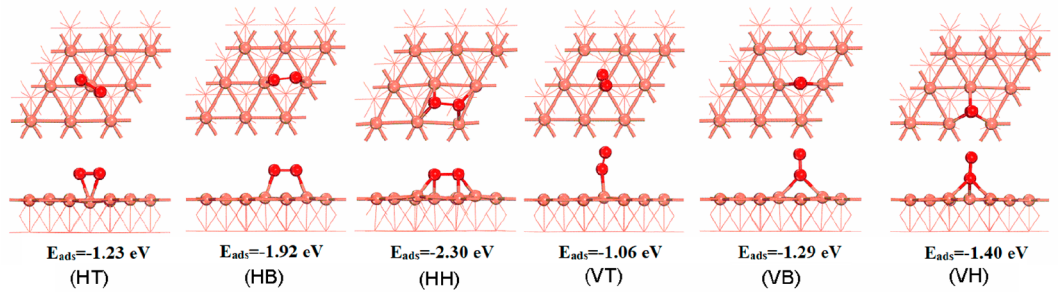

Figure 3. Optimized geometric structures of O_2 adsorption on the Cu(111) surface.

https://dx.doi.org/10.1021/acs.energyfuels.0c00941
Energy Fuels 2020, 34, 8718−8725

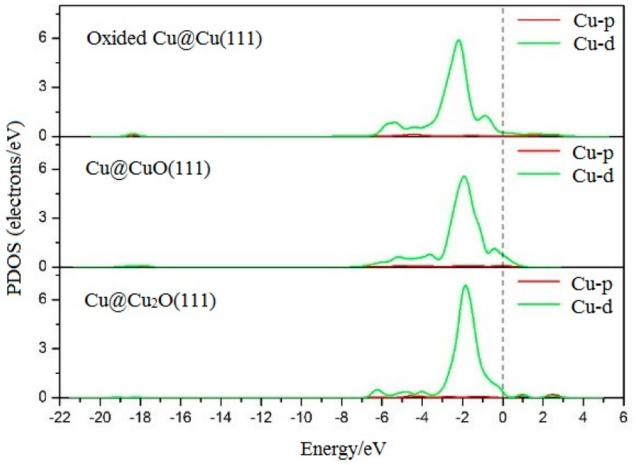

Figure 5. PDOS of Cu atoms (Cu, Cu^{2+}, and Cu^{+}) at different surfaces.

of Cu@CuO(111) rather than Cu@Cu_2O(111) (also as a reference). Additionally, an alternative method of identifying phase transformation is the charge analysis.[48] On the basis of the same set of optimization parameters, the Mulliken charges of the Cu cations in both Cu_2O(111) and CuO(111) bulk models are computed. Calculated results indicate that the Mulliken charge of all of the copper cations in the Cu_2O(111) bulk ranges from 10.6 to 10.8 e, while that of all of the copper cations in the CuO(111) model ranges from 10.2 to 10.5 e. Therefore, the involved copper cation charge of the nano-island is then analyzed [as given by Figure 4 (FS)]. The copper cation bonding with the two oxygen anions possesses a total Mulliken charge of 10.42 e, which means that Cu^0 has been first oxidized to Cu^{2+} rather than Cu^{+}. Therefore, it can be concluded that, at the very initial stage, the surface oxidation of Cu(111) will first form a CuO nano-island above the surface, while the main component in the bulk is still Cu phase, which also partially validates the hypothesis of Zhu et al.[24]

3.2. Subsequent Surface Oxidation of Cu(111): The Formation of an Exterior Thin CuO Layer. After the incipient surface oxidation, a CuO nano-island with high oxygen potential and relatively low copper concentration is formed, which would motivate the growth of the oxide island and then the formation of a thin CuO layer during the further exposure to O_2. There are two potential processes for this evolution. One is the inward diffusion of the surface oxygen atom, and the other is the outward diffusion of the sublayer copper atom. Thus, the final state [Figure 4 (FS)] of the incipient surface oxidation is set as the initial state of both oxygen anion and copper cation diffusions.

At first, the energy profile of oxygen inward diffusion is shown in Figure 6a. The oxygen atom (marked by blue) is moved from the surface to the next layer with an energy barrier of 1.90 eV to break the bonds between this oxygen atom and the surface copper atoms. The reaction energy of this process is 1.78 eV, indicating that plenty of heat is required for the oxygen inward diffusion. It can be observed in Figure 6 (FS) that the migrated oxygen atom bonds with the sublayer copper atoms and then turns to be a four-coordinated structure, which is similar to the standard tetrahedral site residing in the Cu_2O(111) lattice (shown in Figure 6b), indicating the formation of subsurface Cu_2O. Meanwhile, the Mulliken charge of the copper adatom increases from 10.42 to 10.64

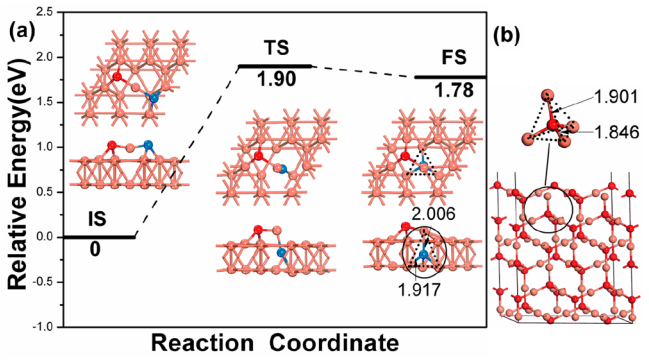

Figure 6. (a) Structures and energy profile of IS, TS, and FS for oxygen inward diffusion in the Cu(111) slab (the diffused O atom is marked blue) and (b) structure of the Cu_2O slab and its tetrahedral site.

e, which also signifies a transformation from Cu^0 to Cu^{+}. Thus, this oxygen inward diffusion process would be a possible mechanism for the initial formation of the Cu_2O phase in the surface.

Furthermore, an investigation about the external diffusion of sublayer copper to the nano-island is carried out as well. The nearest sublayer copper atom (Cu_{sub}) under the surface copper vacancy (V_{Cu}) is first considered; however, after geometry optimization, it is found that Cu_{sub} would prefer to move back to the original site instead of entering the surface layer. This means that the movement of Cu_{sub} to V_{Cu} is rather difficult. Meanwhile, it must be noted that, during a real oxidation process, the high temperature intensifies the vibrations of all atoms and the copper atoms on the same layer around V_{Cu} would also migrate along different orientations. As shown in Figure 7, a neighbor sublayer copper atom (the blue ball)

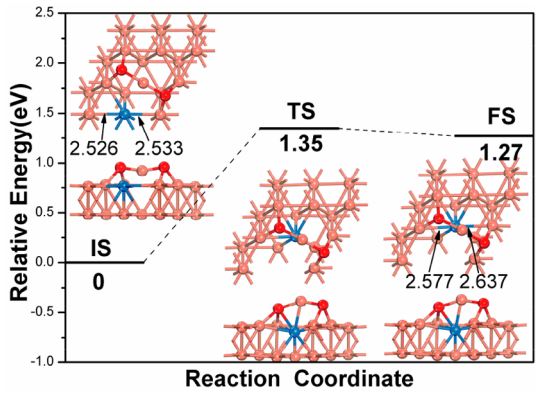

Figure 7. Structures and energy profile of IS, TS, and FS for copper surface diffusion in the Cu(111) slab (the diffused Cu atom is marked blue).

tends to move horizontally to V_{Cu} and little change to the surface copper concentration and less bond cleavage facilitate this surface migration. As a result, the CuO nano-island is lifted farther away from the substrate [Figure 7 (FS)], completely echoing the epitaxial growth mechanism.[29−31]

As seen, the epitaxial growth of the nano-island might mainly be produced by the copper surface diffusion rather than the outward diffusion. Meanwhile, the energy barrier and reaction heat of this horizontal diffusion are 1.35 and 1.27 eV, respectively, and apparently, both of them are lower than those

https://dx.doi.org/10.1021/acs.energyfuels.0c00941
Energy Fuels 2020, 34, 8718−8725

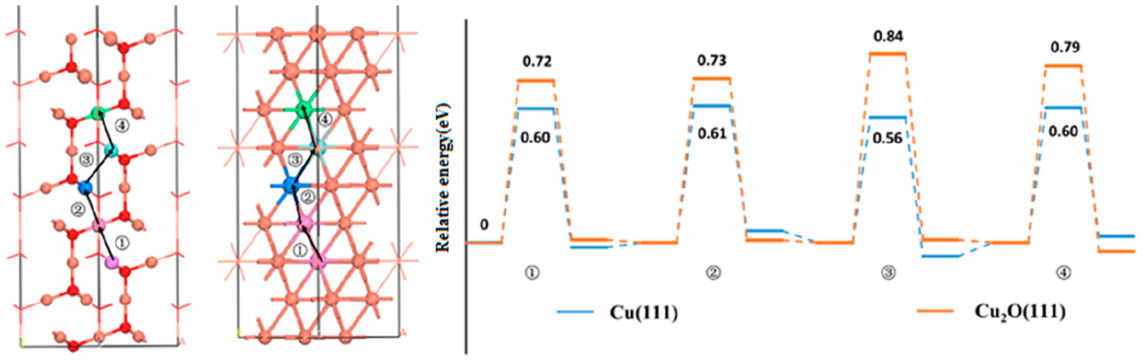

Figure 8. Cu diffusion paths and energy profile with energy barriers in the Cu(111) and Cu_2O(111) bulk (the colorized balls present the diffusion Cu cations).

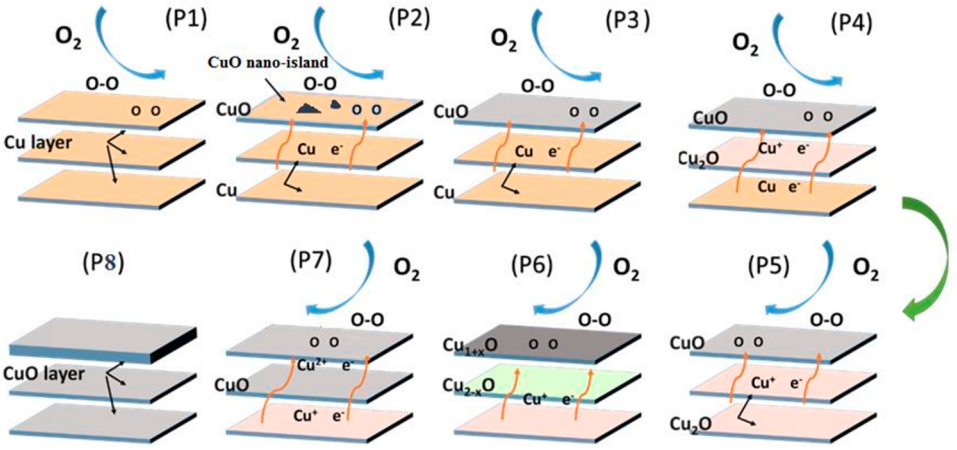

Figure 9. Schematic of the oxidation process of Cu → Cu_2O → CuO.

of oxygen inward diffusion (1.90 and 1.78 eV). Thus, it can be concluded that the copper horizontal diffusion (correspondingly, the CuO nano-island growth) is easier than the oxygen inward diffusion (correspondingly, the sublayer Cu_2O growth). That is, as a result of this subsequent surface oxidation, the growth of the CuO nano-island will lead to the formation of an exterior thin CuO layer above the surface of the Cu(111) bulk as more nano-islands are produced and then grow rather than Cu_2O.

3.3. Bulk Oxidation of Cu(111): The Successive Formation of Cu_2O and CuO in Bulk. The oxide growth during the high-temperature oxidation process requires a continual source of ions.[49] Above DFT calculations indicate that the onset of oxide formation displays a volume expansion (the epitaxial growth of the oxide nano-island), indicating that the "growth source" should be the copper diffusion in the bulk region.[27] As labeled in Figure 8, the outward diffusions of copper atoms from the deep bulk region to upper layer in the nine-layer Cu(111) and Cu_2O(111) slab models are calculated, respectively, and four-step diffusions are considered to adequately describe the diffusion pathways. It is found that the energy barriers for the copper diffusion in the bulk region are close to each other, and the diffusion energies are around 0.6 eV in the Cu(111) bulk, while the diffusion energies are about 0.8 eV in the Cu_2O(111) bulk. The energy barrier of each diffusion step in the Cu(111) bulk is also smaller than that in the Cu_2O(111) bulk, indicating that oxidation (accompanying with the copper outward diffusion) of the Cu(111) bulk is faster than that of Cu_2O(111). It is therefore conjectured that copper oxidation in the Cu(111) bulk (correspondingly, the formation of the Cu_2O phase) precedes that in the Cu_2O(111) bulk (correspondingly, the formation of the CuO phase), and Cu_2O will become the main component in the bulk as metallic copper atoms are entirely consumed. The deduction is also consistent with the thermogravimetric experimental results,[50] in which the oxidation rate of copper would suddenly drop as Cu^0 is converted to Cu^+. Namely, the main component in the bulk changes in the form of Cu → Cu_2O → CuO, while the shell of the bulk would still be the CuO phase. In terms of energy barriers of the whole oxidation process, it can be noted that the energy barrier of the subsequent surface oxidation (1.35 eV) is higher than that of the incipient surface oxidation (0.17 eV) and the bulk oxidation (0.60 eV), indicating that the rate-determined step of the whole oxidation process is the horizontal diffusion of copper atoms on the surface.

3.4. Copper Oxidation Mechanism. The complete Cu oxidation process can be divided into two parts, the surface oxidation and the bulk oxidation, which has already been obtained by the above DFT calculations. Thus, the Cu oxidation mechanism can be summarized briefly: (1) At the initial stage, as shown in Figure 9 (P1), the copper atoms on the gas−solid interface react with O_2 rapidly with a small thermodynamic resistance, producing the CuO nano-islands [Figure 9 (P2)]. (2) As a result of the surface horizontal diffusion of the copper atoms, the CuO nano-island gradually

https://dx.doi.org/10.1021/acs.energyfuels.0c00941
Energy Fuels 2020, 34, 8718−8725

grows, echoing the epitaxial growth of the oxide. An outmost thin CuO layer will be eventually formed on the surface of the Cu(111) bulk as more CuO nano-islands are produced and then grow [as depicted in Figure 9 (P3)]. (3) Next, the sublayer copper atoms will accumulate to the surface to balance the copper concentration gradient between the surface and sublayer. The reaction $Cu + Cu^{2+} + e^- + h^+ \rightarrow 2Cu^+$ brings a Cu_2O layer between the surface CuO layer and interior Cu layer. Along with the surface oxygen uptake reaction, as shown in Figure 9 (P4), the Cu_2O layer grows thicker and more Cu^0 atoms donate electrons, transforming to be Cu^+. (4) When a complete consumption of the metallic copper happens, as shown in Figure 9 (P5), the Cu_2O phase becomes the main component of the OC, while the shell would still be the CuO phase. Hence, the first step of the copper oxidation mechanism of $Cu \rightarrow Cu_2O$ has been obtained.

In combination with our previous research[27] on the Cu_2O oxidation ($Cu_2O \rightarrow CuO$), a complete oxidation mechanism of Cu is then obtained. (5) As shown in Figure 9 (P6), the slightly excessive copper cations within the external $Cu_{1+x}O$ layer continue to react with O_2 molecules quickly, forming a new product layer at the exterior. (6) With the progress of the copper atom outward diffusion, the Cu/O ratio of the "interior layer" approaches 1:1 via $Cu_2O + V_{Cu} \rightarrow CuO$, which leads to the formation of CuO in the bulk phase. As presented in Figure 9 (P7), the external CuO layer becomes thicker and thicker. (7) Finally, with the complete conversion of internal Cu_2O, as shown in Figure 9 (P8), the complete oxidation process of $Cu \rightarrow Cu_2O \rightarrow CuO$ is finished.

3.5. Partial Oxidation Experiment of Pure Copper. To validate the first-step oxidation mechanism of Cu, an isothermal oxidation experiment is performed and the partially oxidized sample can be seen in Figure 2b. As shown in Figure 10, the cross section of the partially oxidized sample is characterized by SEM with a 1000× magnification level. Naturally, it is noted that the microstructure of the partially oxidized sample consists of three layers: the outer thin layer (points 003 and 004), the middle layer (point 002), and the inner layer (point 001), while the outer surface is also covered by abundant oxide islands (marked by the white dotted line frame). The appearance of the nano-islands is in accordance with the simulation results.

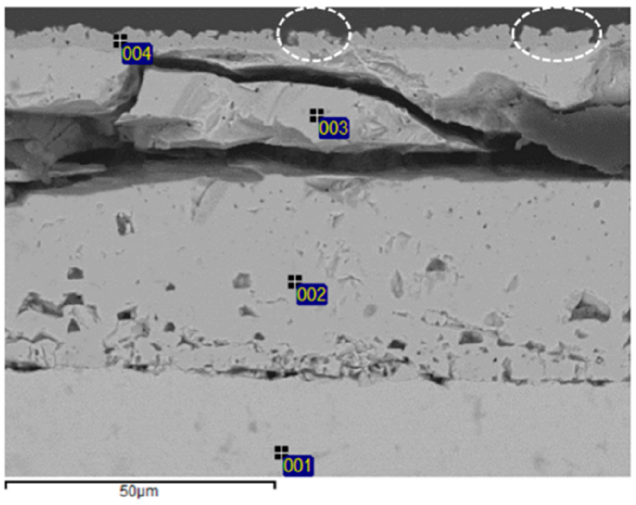

Figure 10. Microstructure of the oxide in copper oxidation at the initial stage (the crannies may result from the different thermal stress in different regions during the temperature-varying period).

Then, these layers are characterized by EDS analysis. In Figure 10 (point 004), there are 20.63 wt % O and 79.37% wt % Cu, which means that the ratio of Cu and O atoms is close to 1:1. That is to say, the outer thin layer must be CuO, which verifies that the oxygen uptake process on the Cu(111) surface would directly produce CuO rather than Cu_2O. Similarly, it is measured that the middle layer (point 002) is Cu_2O (11.97 wt % O and 88.03 wt % Cu). At the same time, the inner layer (point 001) remains copper substrate, while the layer (point 003) is a transition region with the Cu/O molar ratio of 1.68:1. As mentioned above, the oxidation of the Cu surface preferentially produces a layer of CuO at first [Figure 9 (P1) and (P2) and Figure 10 (point 4)] and the growth of Cu_2O is the dominant process in the early stage [Figure 9 (P4) and (P5) and Figure 10 (point 2)]. Consequently, the first-step oxidation mechanism of Cu has been supported by the partial oxidation experiment.

4. CONCLUSION

DFT calculations have been employed to investigate the Cu oxidation mechanism in the CLC process. The whole oxidation process can be divided into two steps: the surface oxidation and the bulk oxidation. First, the most likely oxidation pathways for the six-layer Cu(111) surface are obtained. The interface reaction between OC and air is significantly exothermic [4.56 eV for Cu(111)], and the incipient surface oxidation of Cu(111) would preferentially produce a CuO nano-island but not Cu_2O, which is verified by the Mulliken charge and PDOS analysis of the oxide nano-island. Second, the growth of the oxide nano-island on the surface is then considered. Results indicate that oxygen inward diffusion will lead to the formation of a Cu_2O-liked structure and copper diffusion prefers a horizontal path, corresponding to an epitaxial growth of the nano-island and then the formation of an exterior thin CuO layer. On the basis of the energy barrier analyses, it is concluded that the growth of the nano-island (forming a thin CuO layer) is easier than the oxygen inward diffusion (producing a Cu_2O phase) on the Cu(111) surface with respect to the surface oxidation of Cu. Third, the continuous replenishment process of copper atoms in unreacted bulk is calculated. Results show that the oxidation of the Cu(111) bulk (leading to the formation of the Cu_2O phase) is faster than that of the Cu_2O(111) bulk (leading to the CuO formation), and as a result, Cu_2O will preferentially become the main component in the bulk because metallic copper is entirely consumed. The Cu_2O bulk is oxidized to form the CuO phase eventually. On the basis of these understandings, a complete oxidation mechanism is established and validated by a well-designed partial oxidation experiment.

AUTHOR INFORMATION

Corresponding Author

Haibo Zhao − *State Key Laboratory of Coal Combustion, School of Energy and Power Engineering, Huazhong University of Science and Technology, Wuhan, Hubei 430074, People's Republic of China;* orcid.org/0000-0002-2693-4499; Phone: +86-27-8754-4779, ext. 8208; Email: hzhao@mail.hust.edu.cn; Fax: +86-27-8754-5526

https://dx.doi.org/10.1021/acs.energyfuels.0c00941
Energy Fuels 2020, 34, 8718−8725

Authors

Chaohe Zheng − *State Key Laboratory of Coal Combustion, School of Energy and Power Engineering, Huazhong University of Science and Technology, Wuhan, Hubei 430074, People's Republic of China*

Jie Cao − *State Key Laboratory of Coal Combustion, School of Energy and Power Engineering, Huazhong University of Science and Technology, Wuhan, Hubei 430074, People's Republic of China*

Yongliang Zhang − *State Key Laboratory of Power Systems, Department of Energy and Power Engineering, Tsinghua University, Beijing 100084, People's Republic of China*

Complete contact information is available at: https://pubs.acs.org/10.1021/acs.energyfuels.0c00941

Notes

The authors declare no competing financial interest.

■ ACKNOWLEDGMENTS

This work was founded by the National Key R&D Program of China (2016YFB0600801). The authors gratefully acknowledge the help of Professor Zhenshan Li of Tsinghua University for the valuable discussions on the single-crystal copper oxidation experiment. The staff from the Analytical and Testing Center at Huazhong University of Science and Technology are appreciated for their related experimental analysis.

■ REFERENCES

(1) Xu, L.; Edland, R.; Li, Z.; Leion, H.; Zhao, D.; Cai, N. Cu-modified manganese ore as an oxygen carrier for chemical looping combustion. *Energy Fuels* **2014**, *28* (11), 7085−7092.

(2) Zhao, H.; Tian, X.; Ma, J.; Chen, X.; Su, M.; Zheng, C.; Wang, Y. Chemical looping combustion of coal in China: Comprehensive progress, remaining challenges, and potential opportunities. *Energy Fuels* **2020**, *59* DOI: 10.1021/acs.energyfuels.0c00989.

(3) Li, D.; Xu, R.; Gu, Z.; Zhu, X.; Qing, S.; Li, K. Chemical-looping conversion of methane: A review. *Energy Technol.* **2019**, 1900925.

(4) Zhao, H.; Tian, X.; Ma, J.; Su, M.; Wang, B.; Mei, D. Development of tailor-made oxygen carriers and reactors for chemical looping processes at Huazhong University of Science & Technology. *Int. J. Greenhouse Gas Control* **2020**, *93*, 102898.

(5) Fan, L.-S.; Li, F. Chemical looping technology and its fossil energy conversion applications. *Ind. Eng. Chem. Res.* **2010**, *49* (21), 10200−10211.

(6) Hedayati, A.; Azad, A.-M.; Rydén, M.; Leion, H.; Mattisson, T. Evaluation of novel ceria-supported metal oxides as oxygen carriers for chemical-looping combustion. *Ind. Eng. Chem. Res.* **2012**, *51* (39), 12796−12806.

(7) Deng, G.; Li, K.; Gu, Z.; Zhu, X.; Wei, Y.; Cheng, X.; Wang, H. Synergy effects of combined red muds as oxygen carriers for chemical looping combustion of methane. *Chem. Eng. J.* **2018**, *341*, 588−600.

(8) Wang, B.; Li, H.; Wang, W.; Luo, C.; Mei, D.; Zhao, H. Reaction characteristic investigation of the combined template-method-made $CaSO_4$−Mn_3O_4 mixed oxygen carrier with lignite. *Energy Fuels* **2019**, *33* (9), 8954−8966.

(9) Tian, X.; Su, M.; Zhao, H. Kinetics of redox reactions of CuO@TiO_2−Al_2O_3 for chemical looping combustion and chemical looping with oxygen uncoupling. *Combust. Flame* **2020**, *213*, 255−267.

(10) Lu, C.; Li, K.; Zhu, X.; Wei, Y.; Li, L.; Zheng, M.; Fan, B.; He, F.; Wang, H. Improved activity of magnetite oxygen carrier for chemical looping steam reforming by ultrasonic treatment. *Appl. Energy* **2020**, *261*, 114437.

(11) de Diego, L. F.; Gayán, P.; García-Labiano, F.; Celaya, J.; Abad, A.; Adánez, J. Impregnated CuO/Al_2O_3 oxygen carriers for chemical-looping combustion: Avoiding fluidized bed agglomeration. *Energy Fuels* **2005**, *19* (5), 1850−1856.

(12) Arjmand, M.; Azad, A.-M.; Leion, H.; Lyngfelt, A.; Mattisson, T. Prospects of Al_2O_3 and $MgAl_2O_4$-supported CuO oxygen carriers in chemical-looping combustion (CLC) and chemical-looping with oxygen uncoupling (CLOU). *Energy Fuels* **2011**, *25* (11), 5493−5502.

(13) Deng, G.; Li, K.; Zhang, G.; Gu, Z.; Zhu, X.; Wei, Y.; Wang, H. Enhanced performance of red mud-based oxygen carriers by CuO for chemical looping combustion of methane. *Appl. Energy* **2019**, *253*, 113534.

(14) Mrowec, S.; Stokłosa, A. Oxidation of copper at high temperatures. *Oxid. Met.* **1971**, *3* (3), 291−311.

(15) Milne, R. H.; Howie, A. Electron microscopy of copper oxidation. *Philos. Mag. A* **1984**, *49* (5), 665−682.

(16) Cocke, D. L.; Chuah, G. K.; Kruse, N.; Block, J. H. Copper oxidation and surface copper oxide stability investigated by pulsed field desorption mass spectrometry. *Appl. Surf. Sci.* **1995**, *84* (2), 153−161.

(17) Park, J. H.; Natesan, K. Oxidation of copper and electronic transport in copper oxides. *Oxid. Met.* **1993**, *39* (5), 411−435.

(18) Zhu, Y.; Mimura, K.; Isshiki, M. Oxidation mechanism of copper at 623−1073 K. *Mater. Trans.* **2002**, *43* (9), 2173−2176.

(19) Mimura, K.; Lim, J. W.; Isshiki, M.; Zhu, Y.; Jiang, Q. Brief review of oxidation kinetics of copper at 350 to 1050 °C. *Metall. Mater. Trans. A* **2006**, *37* (4), 1231−1237.

(20) Chuang, S. Y.; Dennis, J. S.; Hayhurst, A. N.; Scott, S. A. Kinetics of the oxidation of a Co-precipitated mixture of Cu and Al_2O_3 by O_2 for Chemical-Looping Combustion. *Energy Fuels* **2010**, *24* (7), 3917−3927.

(21) Hien, V. X.; Kim, S.-Y.; Lee, J.-H.; Kim, J.-J.; Heo, Y.-W. Growth of CuO nanowires on graphene-deposited Cu foil by thermal oxidation method. *J. Cryst. Growth* **2013**, *384*, 100−106.

(22) Maya, J. C.; Chejne, F. Modeling of oxidation and reduction of a copper-based oxygen carrier. *Energy Fuels* **2014**, *28* (8), 5434−5444.

(23) Shi, L.; Wang, R.; Zhai, H.; Liu, Y.; Gao, L.; Sun, J. A long-term oxidation barrier for copper nanowires: Graphene says yes. *Phys. Chem. Chem. Phys.* **2015**, *17* (6), 4231−4236.

(24) Zhu, Y.; Mimura, K.; Isshiki, M. A study of the initial oxidation of copper in 0.1 MPa oxygen and the effect of purity by metallographic methods. *Corros. Sci.* **2004**, *46* (10), 2445−2454.

(25) Zhu, Y.; Mimura, K.; Isshiki, M. Oxidation mechanism of Cu_2O to CuO at 600−1050°C. *Oxid. Met.* **2004**, *62* (3), 207−222.

(26) Grzesik, Z.; Migdalska, M. Oxidation mechanism of Cu_2O and defect structure of CuO at high temperatures. *High Temp. Mater. Processes* **2011**, *30* (4−5), 277−287.

(27) Su, M.; Cao, J.; Tian, X.; Zhang, Y.; Zhao, H. Mechanism and kinetics of Cu_2O oxidation in chemical looping with oxygen uncoupling. *Proc. Combust. Inst.* **2019**, *37*, 4371−4378.

(28) Gattinoni, C.; Michaelides, A. Atomistic details of oxide surfaces and surface oxidation: The example of copper and its oxides. *Surf. Sci. Rep.* **2015**, *70* (3), 424−447.

(29) Xu, Y.; Mavrikakis, M. Adsorption and dissociation of O_2 on Cu(111): Thermochemistry, reaction barrier and the effect of strain. *Surf. Sci.* **2001**, *494* (2), 131−144.

(30) Soon, A.; Todorova, M.; Delley, B.; Stampfl, C. Oxygen adsorption and stability of surface oxides on Cu(111): A first-principles investigation. *Phys. Rev. B: Condens. Matter Mater. Phys.* **2006**, *73* (16), 165424.

(31) Li, A.; Song, H.; Zhou, J.; Chen, X.; Liu, S. CuO nanowire growth on Cu_2O by *in situ* thermal oxidation in air. *CrystEngComm* **2013**, *15* (42), 8559.

(32) Jeon, B.; Sankaranarayanan, S. K. R. S.; van Duin, A. C. T.; Ramanathan, S. Influence of surface orientation and defects on early-stage oxidation and ultrathin oxide growth on pure copper. *Philos. Mag.* **2011**, *91* (32), 4073−4088.

(33) Volker, E.; Williams, F. J.; Calvo, E. J.; Jacob, T.; Schiffrin, D. J. O_2 induced Cu surface segregation in Au-Cu alloys studied by angle resolved XPS and DFT modelling. *Phys. Chem. Chem. Phys.* **2012**, *14* (20), 7448−7455.

(34) Saidi, W. A.; Lee, M.; Li, L.; Zhou, G.; McGaughey, A. J. H. *Ab initio* atomistic thermodynamics study of the early stages of Cu(100) oxidation. *Phys. Rev. B: Condens. Matter Mater. Phys.* **2012**, *86* (24), 3789−3797.
(35) Kangas, T.; Laasonen, K. Formation of a missing row reconstruction on a Cu(100) surface: An atom scale density functional theory based study. *Surf. Sci.* **2012**, *606* (3), 192−201.
(36) Ma, L.; Zhang, J.; Xu, K. Structural and electronic properties of atomic oxygen adsorption on Cu(111) surface: A first-principles investigation. *Sci. China: Phys., Mech. Astron.* **2013**, *56* (3), 573−580.
(37) Zhang, Y.; Zhao, H.; Guo, L.; Zheng, C. Decomposition mechanisms of Cu-based oxygen carriers for chemical looping with oxygen uncoupling based on density functional theory calculations. *Combust. Flame* **2015**, *162* (4), 1265−1274.
(38) Zhao, H.; Zhang, Y.; Wei, Y.; Gui, J. Understanding CuO-support interaction in Cu-based oxygen carriers at a microcosmic level. *Proc. Combust. Inst.* **2017**, *36* (3), 4069−4077.
(39) Qin, W.; Wang, Y.; Lin, C.; Hu, X.; Dong, C. Possibility of morphological control to improve the activity of oxygen carriers for chemical looping combustion. *Energy Fuels* **2015**, *29* (2), 1210−1218.
(40) Tian, D.; Li, K.; Wei, Y.; Zhu, X.; Zeng, C.; Cheng, X.; Zheng, Y.; Wang, H. DFT insights into oxygen vacancy formation and CH_4 activation over CeO_2 surfaces modified by transition metals (Fe, Co and Ni). *Phys. Chem. Chem. Phys.* **2018**, *20* (17), 11912−11929.
(41) Perdew, J. P.; Chevary, J. A.; Vosko, S. H.; Jackson, K. A.; Pederson, M. R.; Singh, D. J.; Fiolhais, C. Atoms, molecules, solids, and surfaces: Applications of the generalized gradient approximation for exchange and correlation. *Phys. Rev. B: Condens. Matter Mater. Phys.* **1992**, *46* (11), 6671−6687.
(42) Vanderbilt, D. Soft self-consistent pseudopotentials in a generalized eigenvalue formalism. *Phys. Rev. B: Condens. Matter Mater. Phys.* **1990**, *41* (11), 7892−7895.
(43) Anisimov, V. I.; Zaanen, J.; Andersen, O. K. Band theory and mott insulators: Hubbard U instead of stoner I. *Phys. Rev. B: Condens. Matter Mater. Phys.* **1991**, *44* (3), 943−954.
(44) Zheng, C.; Zhao, H. Exploring the microscopic reaction mechanism of H_2S and COS with CuO oxygen carrier in chemical looping combustion. *Fuel Process. Technol.* **2020**, *205*, 106431.
(45) Fehrenbach, G. M.; Bross, H. Self-consistent spline augmented-plane-wave calculation: Ground-state properties of Cu. *Phys. Rev. B: Condens. Matter Mater. Phys.* **1993**, *48* (24), 17703−17714.
(46) Kirfel, A.; Eichhorn, K. Accurate structure analysis with synchrotron radiation. the electron density in Al_2O_3 and Cu_2O. *Acta Crystallogr., Sect. A: Found. Crystallogr.* **1990**, *46* (4), 271−284.
(47) Govind, N.; Petersen, M.; Fitzgerald, G.; King-Smith, D.; Andzelm, J. A generalized synchronous transit method for transition state location. *Comput. Mater. Sci.* **2003**, *28* (2), 250−258.
(48) Maimaiti, Y.; Nolan, M.; Elliott, S. D. Reduction mechanisms of the CuO(111) surface through surface oxygen vacancy formation and hydrogen adsorption. *Phys. Chem. Chem. Phys.* **2014**, *16* (7), 3036−3046.
(49) Qin, L.; Cheng, Z.; Fan, J. A.; Kopechek, D.; Xu, D.; Deshpande, N.; Fan, L.-S. Nanostructure formation mechanism and ion diffusion in iron−titanium composite materials with chemical looping redox reactions. *J. Mater. Chem. A* **2015**, *3* (21), 11302−11312.
(50) Prisedsky, V. V.; Vinogradov, V. M. Fragmentation of diffusion zone in high-temperature oxidation of copper. *J. Solid State Chem.* **2004**, *177* (11), 4258−4268.

■ NOTE ADDED AFTER ASAP PUBLICATION

This paper was published ASAP on May 26, 2020, with an incorrect DOI for reference 2. The corrected version was posted on May 27, 2020.

https://dx.doi.org/10.1021/acs.energyfuels.0c00941
Energy Fuels 2020, 34, 8718−8725